CMS Physics Analysis Summary

Contact: cms-pag-conveners-susy@cern.ch 2015/03/23

Search for supersymmetry with the vector boson fusion topology in proton-proton collisions at $\sqrt{s} = 8$ TeV

The CMS Collaboration

Abstract

The first search for supersymmetry with the vector boson fusion (VBF) topology is presented. The VBF topology offers a promising avenue to study the electroweak sector of supersymmetry. The search targets final states with at least two leptons, large missing transverse momentum, and two jets with a large pseudorapidity gap. The data sample used in this analysis corresponds to an integrated luminosity of 19.7 fb^{-1} of pp collisions at $\sqrt{s} = 8$ TeV collected with the CMS detector. The observed dijet invariant mass spectrum after the final selections is consistent with the expected standard model predictions. Upper limits are set for the production of charginos and neutralinos with two associated jets, where sleptons are ligher than charginos.

1 Introduction

With the spectacular performance of the LHC machine, a host of results from the ATLAS and CMS experiments have constrained a large number of new physics scenarios beyond the standard model (SM). In particular, both experiments have placed bounds over 1 TeV on the masses of the gluino ($\tilde{g}$) and the squarks ($\tilde{q}$) of the first two generations in models of supersymmetry (SUSY) [1–5]. On the other hand, the chargino ($\tilde{\chi}_i^{\pm}$) and neutralino ($\tilde{\chi}_i^0$) masses are less constrained, especially in compressed mass-spectra scenarios, as expected in a hadron collider where these particles suffer from smaller electroweak production cross sections. The chargino-neutralino sector plays a crucial role in the dark matter (DM) connection of SUSY models. The lightest neutralino, $\tilde{\chi}_1^0$, as the lightest supersymmetric particle (LSP), is the dark matter candidate in R-parity conserving SUSY extensions of the SM.

ATLAS and CMS have dedicated searches for direct production of charginos and neutralinos in final states with one or more leptons and $E_{\mathrm{T}}^{\mathrm{miss}}$ [6, 7], e.g. $\tilde{\chi}_1^{\pm}\tilde{\chi}_2^0 \to \ell\ell\ell\nu\tilde{\chi}_1^0\tilde{\chi}_1^0$. However, the searches exhibit limited sensitivity in cases where the $\tilde{\chi}_1^{\pm}$ and the next-to-lightest neutralino, $\tilde{\chi}_2^0$, are nearly mass degenerate with the $\tilde{\chi}_1^0$. The mass separation $\Delta m = m_{\tilde{\chi}_1^{\pm}} - m_{\tilde{\chi}_1^0}$ is an important factor in the exclusion plots from both experiments. While the exclusion limits can be as high as $m_{\tilde{\chi}_1^{\pm}} < 720$ GeV for $m_{\tilde{\chi}_1^0} = 0$ GeV, the bounds on $m_{\tilde{\chi}_1^{\pm}}$ are ~ 100 GeV for $\Delta m < 50$ GeV. Additionally, models with large branching ratios to τ leptons suffer from more modest exclusion limits, even in the scenario where $m_{\tilde{\chi}_1^0} = 0$ GeV, due to the larger τ misidentication rates which make it difficult to manage the level of backgrounds.

DM and electroweak sparticles can be pair produced in association with two jets in pure electroweak processes at the LHC [8]. This paper describes a search for pair production of electroweak SUSY particles with two associated jets using the vector boson fusion (VBF) topology, which is characterized by the presence of two jets in the forward direction, in opposite hemispheres of the CMS detector, and with large dijet invariant mass (m_{jj}). The VBF topology offers a new complimentary route to directly probe the electroweak sector of SUSY, especially in compressed mass-spectra scenarios [9] and/or final states which suffer significantly larger contamination from strongly produced SM backgrounds. Because the cross section for electroweak SUSY production is expected to be small compared to the SM backgrounds with similar topology, another strategy to search for DM and electroweak SUSY focuses on cascade decays of heavy colored particles such as gluinos and squarks, which have larger expected production cross sections. For example, a decay chain such as $\tilde{q}\tilde{q} \to qq\tilde{\chi}_2^0\tilde{\chi}_2^0 \to qq\tau\tau\tilde{\tau}\tilde{\tau} \to qq\tau\tau\tau\tau\tilde{\chi}_1^0\tilde{\chi}_1^0$ leads to a signature with missing energy ($E_{\mathrm{T}}^{\mathrm{miss}}$), multiple jets and leptons. However, in a scenario where colored objects are heavy and the production cross section is too small to be accessible at the LHC, the VBF topology provides a unique opportunity to target uncharted parts of the SUSY phase space, where other experimental searches have limited sensitivity. Searching for SUSY with VBF jets is reminiscent of probes using cascade decays, in the sense that jets with relatively high transverse momentum (p_T) are used to reduce the SM non-VBF background rates. Thus, the highly energetic jets of usual SUSY searches are used, but without requiring the productions of squark and gluinos with subsequent decay chains.

The search targets final states with the VBF topology and with at least two reconstructed leptons with like-sign (LS) or opposite-sign (OS) electric charge. It makes use of eight independent final states: $\mathrm{e}^{\pm}\mu^{\pm}jj$, $\mathrm{e}^{\pm}\mu^{\mp}jj$, $\mu^{\pm}\mu^{\pm}jj$, $\mu^{+}\mu^{-}jj$, $\mu^{\pm}\tau_h^{\pm}jj$, $\mu^{\pm}\tau_h^{\mp}jj$, $\tau_h^{\pm}\tau_h^{\pm}jj$, and $\tau_h^{+}\tau_h^{-}jj$ where the symbol τ_h is used to indicate a reconstructed hadronic decay of a τ lepton and 'j' is used to indicate a VBF tagged jet. The analysis is performed using data collected with the CMS detector in proton-proton collisions at a centre of mass energy of $\sqrt{s} = 8$ TeV at the LHC. The data samples correspond to an integrated luminosity of 19.7 fb^{-1}.

The invariant mass shape of the leading dijet candidate passing VBF topological selections is used to fit for a potential excess in data and determine the sensitivity of the analysis. In the case of SUSY, the production of charginos and neutralinos occur in pairs and thus the VBF tagged jets have a higher average transverse momentum than in VBF Higgs searches [10–12], which allows for more stringent VBF requirements to reduce the background rates by $\sim 10^{-2}$-10^{-4}, depending on the background. In addition to VBF requirements, a relatively high $E_{\mathrm{T}}^{\mathrm{miss}}$ requirement is imposed due to the presence of the LSPs. These more stringent VBF requirements and relatively large $E_{\mathrm{T}}^{\mathrm{miss}}$ cuts also suppress the SM backgrounds produced through vector boson fusion, such as VBF Higgs/Z.

The background contributions in the signal region are predicted using data wherever possible. The general strategy is to modify the standard selection requirements to select multiple control region samples dominated by each background process. These control regions are used to measure the m_{jj} shapes and probabilities for background candidates to pass the VBF selection requirements. If the background contributions are small and/or the above approach is not feasible, the m_{jj} shapes are taken from simulation. In these cases, scale factors, defined as the ratio of efficiencies measured in data and simulation, are used to normalize the predicted rates to the data by correcting the expected contributions obtained from the simulation samples.

The paper is organized as follows. The CMS detector is described in section 2, while the reconstruction of electrons, muons, τ_h, jets, and $E_{\mathrm{T}}^{\mathrm{miss}}$ are described in section 3. The dominant backgrounds and their Monte-Carlo (MC) simulated samples are described in section 4, followed by the description of event selections in section 5 and the background estimation in section 6. Finally, systematic uncertainties are summarized in section 7 and the results are presented in section 8.

2 CMS Detector

The CMS experiment [13] uses a right-handed coordinate system, with the origin at the nominal interaction point, the x axis pointing to the centre of the LHC ring, the y axis pointing up (perpendicular to the LHC plane), and the z axis along the anticlockwise-beam direction. The polar angle, θ, is measured from the positive z axis and the azimuthal angle, ϕ, is measured in the x-y plane. The pseudorapidity is given by $\eta = -\ln\tan(\theta/2)$.

The central feature of the CMS apparatus is a superconducting solenoid of 6 m inner diameter, providing a field of 3.8 T. Within the field volume are the silicon pixel and strip tracker, the crystal electromagnetic calorimeter (ECAL), which includes a silicon sensor preshower detector in front of the ECAL endcaps, and the brass/scintillator hadron calorimeter (HCAL). Muons are measured in gas-ionization detectors embedded in the steel return yoke. In addition to the barrel and endcap detectors, CMS has extensive forward calorimetry.

The inner tracker measures charged particles within $|\eta| < 2.5$ and provides an impact parameter resolution of ~ 15 μm and a transverse momentum resolution of about 1.5 % for 100 GeV particles. Collision events are selected by a first level trigger made of a system of fast electronics and a higher level trigger that consists of a farm of commercial CPUs running a version of the offline reconstruction optimized for fast processing. A more detailed description of the CMS detector can be found elsewhere [13].

3 Object Reconstruction and Identification

The jets and the transverse momentum imbalance in the detector ($E_{\mathrm{T}}^{\mathrm{miss}}$) are reconstructed with the Particle Flow (PF) algorithm [14]. The anti-k_T clustering algorithm [15] with $R = 0.5$ is used for jet clustering. Jets are required to pass identification criteria designed to reject particles from pileup interactions and anomalous behavior from the calorimeters. For jets with $p_{\mathrm{T}} > 30$ GeV and $|\eta| < 2.5$ (> 2.5), the identification efficiency is $\approx 99\%$ (95%), while 90–95% (60%) of pileup jets are rejected [16]. The jet energy scale and resolution is calibrated through correction factors that depend on the p_T and η of the jet [17]. Jets originating from the hadronization of bottom quarks are identified using the loose working point of the combined secondary vertex (CSV) algorithm [18] which exploits observables related to the long lifetime of b hadrons. For b-quark jets with $p_{\mathrm{T}} > 20$ GeV and $|\eta| < 2.4$, the identification efficiency is $\approx 85\%$ with a $\approx 10\%$ fake rate for light quark and gluon jets [19].

Muons are reconstructed using the tracker and muon chambers. Quality cuts based on the minimum number of hits in the silicon tracker, pixel detector and muon chambers are applied to suppress backgrounds from decays in flight and hadron shower remnants that reach the muon system [20]. Electrons are reconstructed by combining tracks produced by the Gaussian Sum Filter algorithm with ECAL clusters. Requirements on the track quality, the shape of the energy deposits in the electromagnetic calorimeter, and the compatibility of the measurements from the tracker and the electromagnetic calorimeter are imposed to distinguish prompt electrons from charged pions and from electrons produced by photon conversions [21]. The electron and muon candidates are required to pass isolation criteria in order to reject misidentified leptons from jets. Isolation is defined as the sum of the p_{T} of the reconstructed charged and neutral particles, within a cone of radius $\Delta R = \sqrt{(\Delta\eta)^2 + (\Delta\phi)^2} = 0.4$ centered around the e/μ track. In both cases the contribution from the e/μ candidate is removed from the sum. Muon identification efficiency is $\approx 95\%$ for muons with $p_{\mathrm{T}} > 15$ GeV and $|\eta| < 2.1$ [22]. The misidentification rate of $\pi^{\pm} \to \mu$ for pions with $p_{\mathrm{T}} > 10$ GeV and $|\eta| < 2.1$ is $\approx 1 \times 10^{-3}$ [23]. Electron identification plus isolation efficiency is 85% (80%) for electrons with $p_{\mathrm{T}} > 30$ GeV in the barrel (endcaps) region [24]. The $j \to e$ misidentification rate is $\approx 5 \times 10^{-3}$ for jets with the kinematic properties described above.

Hadronic decays of the τ lepton are reconstructed and identified using the hadrons plus strips (HPS) algorithm [25] designed to optimize the performance of τ_h reconstruction by considering specific τ_h decay modes. To suppress backgrounds in which light-quark or gluon jets can mimic hadronic taus, a τ_h is required to be spatially isolated from other energy in the event. The isolation variable is calculated using a multivariate *Boosted Decision Tree* (BDT) technique by forming rings of radius ΔR in the vicinity of the identified τ_h and using the energy deposits of particles not considered in the reconstruction of the τ_h decay mode and the energy density ρ in the event. Additionally, τ_h candidates are also required to be distinguishable from electrons and muons in the event by using dedicated criteria based on the consistency between the measurements in the tracker, calorimeters, and muon detectors. The identification and isolation efficiency is $\approx$ 55–65% for a τ_h with $p_{\mathrm{T}} > 20$ and $|\eta| < 2.1$. The $j \to \tau_h$ misidentification rate is $\approx$ 1–5% [26], depending on p_{T} and η.

4 Signal and Background Samples

The background composition depends on the channel and, in particular, on the number of τ_hs in the final state. The most important sources of background are the production of W/Z bosons in association with jets (W/Z + jets), $t\bar{t}$, dibosons (WW, WZ), and QCD multijet production. The

W + jets events are characterized by an isolated lepton from the decay of the W boson and uncorrelated jets misidentified as an e, μ or τ_h. Since the misidentification rate for a τ_h is larger than for electrons and muons, W + jets production is particularly relevant in the channels with one τ_h. Background from $t\bar{t}$ events is usually accompanied by one or two b-quark jets, in addition to genuine isolated e, μ or τ_h. Background from diboson events produces both genuine, isolated leptons, when the gauge bosons decay leptonically, and a misidentified τ_h when they decay hadronically. Finally, QCD events are characterized by jets which can be misidentified as charged e, μ and τ_h. The QCD multijets process is only an appreciable background in the $\tau_h\tau_h$ channel.

Collision data are compared to samples of Monte-Carlo simulated events. The signal event samples are generated with the MADGRAPH program (v5.1.5)[27], considering pair production of $\tilde{\chi}_1^{\pm}$ and $\tilde{\chi}_2^0$ ($\tilde{\chi}_1^{\pm}\tilde{\chi}_1^{\pm}$, $\tilde{\chi}_1^{\pm}\tilde{\chi}_1^{\mp}$, $\tilde{\chi}_1^{\pm}\tilde{\chi}_2^0$ and $\tilde{\chi}_2^0\tilde{\chi}_2^0$) with two associated partons. The signal events are generated with the requirement of $p_T > 30$ GeV on both partons and a pseudorapidity gap of $\Delta\eta > 4.2$. The background event samples with a Higgs boson produced through VBF are generated with the POWHEG program (v1.0r1380) [28]. The MADGRAPH generator (v5.1.3) is used for DY + jets, W + jets, $t\bar{t}$ + jets, and diboson production. All MC samples incorporate the CTEQ6L1 or CTEQ6M parton distribution functions. The POWHEG and MADGRAPH generators are interfaced with PYTHIA (v6.4.22) [29] for parton shower and fragmentation. The τ-lepton decays have been performed with TAUOLA [30]. The generated background samples are processed with a detailed simulation of the CMS apparatus using the GEANT4 package [31], while the response for signal samples is modeled with the CMS fast simulation program [32]. For the signal acceptance and m_{jj} shapes based on the fast simulation, the differences with respect to the GEANT4-based results are found to be small ($< 5\%$). Corrections are applied to account for the differences. The MC background and signal yields are normalized to integrated luminosity using next-to-next-leading order (NNLO) and leading order (LO) cross-sections respectively. In all MC samples, multiple interactions are superimposed on the primary collision process, and events are reweighted such that the distribution of reconstructed collision vertices matches that in data (mean=21 and RMS=5.5).

5 Event Selection

A single muon trigger [20] with a p_T threshold of 24 GeV is used for the $\mu\mu jj$, $e\mu jj$, and $\mu\tau_h jj$ final states. The $\tau_h\tau_h jj$ channels use a double-hadronic τ trigger [33] which has a p_T threshold of 35 GeV. A requirement on pseudorapidity ($|\eta| < 2.1$) is applied to select high quality reconstructed and well isolated leptons (e, μ, τ_h) within the tracker acceptance. The p_T thresholds defining the search regions are chosen to achieve a trigger efficiency greater than 90%. For final states with a muon ($\mu\mu jj, e\mu jj, \mu\tau_h jj$), events are selected by requiring $p_T(\mu) > 30$ GeV. In the case of final states with at least two τ_h candidates, the threshold on the $p_T(\tau_h)$ is set to 45 GeV.

The following requirements, referred to as the "central selection", are applied for all final states. Pairs of leptons are required to be separated by $\Delta R > 0.3$. Events with a e/μ are required to have at least 75 GeV of missing transverse energy ($E_{\mathrm{T}}^{\mathrm{miss}} > 75$ GeV), while a cut of $E_{\mathrm{T}}^{\mathrm{miss}} > 30$ GeV is required for the $\tau_h\tau_h jj$ final state to compensate for the loss in acceptance due to the higher τ_h p_T threshold. The contribution from $t\bar{t}$ events is minimized by selecting events where none of the jets have been identified as b-quark jets using the loose working point of the CSV algorithm. Only jets with p_T greater than 20 GeV and separated from the leptons by $\Delta R > 0.3$ are searched for b-quark jets.

The *VBF selection* refers to the requirement of at least two jets with large separation in η ($\Delta\eta > 4.2$), and in opposite hemispheres ($\eta_1 \times \eta_2 < 0$). Events are selected with at least two jets with

$p_T > 50$ GeV and pseudorapidity $|\eta| < 5.0$. The $\mu^{\pm}\mu^{\pm}jj$ search region has a lower background rate with respect to other final states, which makes it possible to relax the jet p_T requirement to 30 GeV to regain signal acceptance. The event selection criteria with $p_T > 30$ GeV used in the $\mu^{\pm}\mu^{\pm}jj$ channel, will be referred to as "Loose". The event selection criteria with $p_T > 50$ GeV used in the $\mu^{\pm}\mu^{\mp}jj$ channel, will be referred to as "Tight". Selected events are required to have a dijet candidate with $m_{jj} > 250$ GeV.

The set of events satisfying the central and VBF selections described above define the signal region (SR). We use the background shapes normalized to the values obtained from the background estimation methods (section 6) to search for a broad enhancement in the tails of the observed m_{jj} spectrum, where simulation predicts an important contribution from a potential signal.

6 Background Estimation

The general methodology used for the estimation of the background contributions in the signal region (SR) is the same for all final states. Mismodeling of the background rate and m_{jj} shape in the simulation may arise from the VBF selection criteria. Therefore, the estimate of the background contribution is determined by isolating various control regions (CRs) to measure the VBF efficiencies (probability for a given background to satisfy the VBF selection criteria) and m_{jj} shapes from data, validate the correct modelling of the central selections and optionally determine a correction factor for the efficiency of the selections by assessing the level of agreement between data and simulation. The VBF efficiency, measured in a CR satisfying only the central selection, is defined as the fraction of events in the CR additionally passing the VBF event selection criteria. For backgrounds estimated entirely from data, the following equation is used to determine their contribution to the signal region:

$$N_{\mathrm{BG}}^{\mathrm{Data}} = N_{\mathrm{BG}}^{\mathrm{MC}}(\mathrm{central}) \cdot SF_{\mathrm{central}}^{\mathrm{CR1}} \cdot \epsilon_{\mathrm{VBF}}^{\mathrm{CR2}}(m_{jj}) \tag{1}$$

where $N_{\mathrm{BG}}^{\mathrm{Data}}$ is the predicted background yield in the signal region, $N_{\mathrm{BG}}^{\mathrm{MC}}(\mathrm{central})$ the predicted rate in simulation without the VBF selections, $SF_{\mathrm{central}}^{\mathrm{CR1}}$ the data-to-simulation correction factor for the central selection as determined from the control sample, and $\epsilon_{\mathrm{VBF}}^{\mathrm{CR}}$ the VBF efficiency, as a function of m_{jj}, determined directly from data.

The event selection criteria used to obtain the CR must not bias the m_{jj} distribution. This is checked, in simulation and data, by comparing the m_{jj} distributions with and without the selection criteria used to obtain the CR. The background estimation technique used to measure the VBF efficiency and m_{jj} shape from data is performed with simulated events to test the closure of the method. The closure tests performed with the MC simulated samples show that the background estimation methods, described in more detail below, are able to reproduce the predicted rate and shape within the statistical uncertainties of the samples, which are propagated as systematic uncertainties on the data-driven measurements of the VBF efficiency. An additional systematic uncertainty, resulting from the difference in the nominal yields and predicted rates from the closure test in simulation, is assigned to the background expectation. The simulated background samples are used to check that the CRs contain the same kinematics and composition of fakes as the signal region so that the scale factors ($SF_{\mathrm{central}}^{\mathrm{CR1}}$) are not biased and can be used to correct the prediction from simulation in the signal region using the method outlined by Equation 1.

The production of $t\bar{t}$ events is an important source of background for the $\mu\mu jj$, $e\mu jj$, and $\mu\tau_h jj$

final states. Control regions enriched with $t\bar{t}$ events are obtained by requiring the presence of at least one reconstructed b-quark jet with $p_T > 20$ GeV. These control samples are used to extract $SF^{\text{CR1}}_{\text{central}}$, which have measured values consistent with unity to the level of $< 3\%$ for the OS channels. The $t\bar{t}$ events with OS lepton pairs are from genuine isolated leptons produced by leptonic decays of W bosons, and thus are well modelled by simulation. On the other hand, $t\bar{t}$ events with LS lepton pairs mostly contain one misidentified lepton, which can be mismodeled in simulation. The data-to-simulation correction factors for central selections in the LS channels range from 1.23 to 1.49 with statistical uncertainties $< 25\%$. The VBF efficiency is measured in samples obtained by additionally removing the charge requirement on the lepton pair and utilizing the lepton isolation sidebands in order to enhance the purity and statistics in the CR. Figure 3(a) shows the "Tight" and ""Loose" VBF efficiencies measured from data, as a function of m_{jj}, for events in the $t\bar{t}$ CRs of the $\mu\mu jj$ final states. The VBF efficiency, $\epsilon^{\text{CR}}_{\text{VBF}}$, has measured values of 1-2%, with relative uncertainties of $< 11\%$, for $m_{jj} > 250$ GeV. The b-jet, charge, and isolation requirements used to obtain the CRs are checked to not bias the m_{jj} shape nor the kinematic distributions of leptons.

The production of W + jets only presents an important source of background for the $\mu\tau_h jj$ search channels. Samples enriched in W + jets events, approximately 70% according to simulation, are obtained by requiring the transverse mass of the lepton and $E_{\text{T}}^{\text{miss}}$ system to be between 40 and 110 GeV. The correction factor $SF^{\text{CR1}}_{\text{central}}$ is measured to be 0.90 ± 0.11, where the total uncertainty is a combination of the statistical uncertainty from data and simulation, as well as the systematic uncertainty arising from the subtraction of the other backgrounds. The lepton and τ_h isolation sidebands are used to obtain additional W + jets enriched samples, with negligible signal contamination, to provide further validation of $SF^{\text{CR1}}_{\text{central}}$ and measure the VBF efficiency and m_{jj} shape directly from data. To validate the measured correction factor, the W + jets rate in the τ_h isolation sideband is scaled by 0.90 ± 0.11. The observed agreement between data and the corrected W + jets rate validates the measured correction factor. The VBF efficiency has a measured value of $7.37 \pm 0.50\%$, where total uncertainty is a combination of the statistical uncertainty from data and the systematic uncertainty arising from the subtraction of the other backgrounds.

The contribution from diboson (VV: WW/WZ/ZZ) events is significant for final states containing only electrons and/or muons, composing up to 10% of the total SM background rate in the OS channels, and up to 40% in the LS channels. This background has genuine isolated leptons and real $E_{\text{T}}^{\text{miss}}$ from neutrinos in addition to associated initial state radiation jets which pass the VBF selections. The VBF efficiency, m_{jj} shape, and the level of agreement between simulation and data in an enriched CR with VV events is expected to be the same for any type of VV production. In a diboson enriched control sample, obtained by requiring at least three leptons and inverting the $E_{\text{T}}^{\text{miss}}$ requirement ($E_{\text{T}}^{\text{miss}} < 75$ GeV), the data-to-simulation correction factor is measured to be 1.12 ± 0.06. The m_{jj} distributions are consistent between data and MC. Therefore, the VBF efficiency is taken directly from simulation.

Control samples dominated by $Z \rightarrow$ee/$\mu\mu$ + jets background events are obtained by utilizing the low $E_{\text{T}}^{\text{miss}}$ sideband and requiring an OS lepton pair having $m_{\ell\ell}$ consistent with the Z boson mass ($m_{\ell\ell}$ between 60 and 120 GeV), where ℓ is e or μ. These control samples (CR1) are used to determine $SF^{\text{CR1}}_{\text{central}}$ and measure from data the shape and normalization of the m_{jj} distribution. The rates and kinematic distributions of leptons in these control samples are consistent between data and MC, with measured data-to-simulation scale factors consistent with unity at the level of $< 1\%$. Figure 3(a) shows the "Tight" and ""Loose" VBF efficiencies measured from data, as a function of m_{jj}, for events in the Z + jets CRs of the $\mu\mu jj$ final states. The level of agreement between simulation and the data-driven measurements of the VBF efficiency is $< 23\%$, which

is treated as a systematic uncertainty on the Z + jets background prediction in the signal region as well as the VBF efficiency in the simulated signal samples. Additional orthogonal Z + jets control samples (CR2) are selected with similar selections to the signal region, maintaining the $E_{\mathrm{T}}^{\mathrm{miss}}$ requirement, and inverting the VBF selections (*i.e.* at least one of the VBF selections are not satisfied: ≥ 2 jets, jet p_T, $\Delta\eta$, or $\eta_1 \cdot \eta_2$). These control samples are used extract correction factors, $SF^{CR2}_{E_{\mathrm{T}}^{\mathrm{miss}}}$, to correct the modeling of high $E_{\mathrm{T}}^{\mathrm{miss}}$ events in the simulation by assessing the level of agreement with data. The mismodeling of the $E_{\mathrm{T}}^{\mathrm{miss}}$ results from the mismeasurement of the p_T of jets and leptons. The observed yields in each control sample are compared with the expected contributions as determined from the simulation and are found to be in agreement. The contribution of $Z \to \ell\ell$ + jets events in the signal regions is estimated using Equation 2.

$$N^{\mathrm{signal}}_{Z\to\ell\ell+\mathrm{jets}} = N^{\mathrm{MC}}_{Z\to\ell\ell+\mathrm{jets}}(\mathrm{central}) \cdot SF^{\mathrm{CR1}}_{\mathrm{central}} \cdot SF^{\mathrm{CR2}}_{E_{\mathrm{T}}^{\mathrm{miss}}} \cdot \epsilon^{\mathrm{CR1}}_{\mathrm{VBF}}(m_{jj}) \tag{2}$$

Finally, high-purity samples of Z$\to \tau\tau$ events in which $SF^{\mathrm{CR1}}_{\mathrm{central}}$ can be evaluated for the search channels with at least one τ_h are obtained by removing the VBF selections and requiring $m_T(\ell, E_{\mathrm{T}}^{\mathrm{miss}})$ < 15 GeV. The VBF efficiency for $Z \to \tau\tau$ + jets processes are obtained from data using the W + jets and $Z \to$ee/$\mu\mu$ + jets control samples described above.

The QCD multijet contribution is negligible in all search channels except the $\tau_h\tau_h jj$ final states. Both the OS and LS search channels estimate the QCD multijet rate in their respective signal regions using LS control regions with $> 90\%$ purity of QCD events. For the OS channel, the QCD multijet background is estimated using Equation 3.

$$N^{\mathrm{signal}}_{\mathrm{QCD}} = N^{\mathrm{CR1}}_{\mathrm{QCD}}(\mathrm{central}) \cdot R_{\mathrm{OS/LS}} \cdot \epsilon^{\mathrm{CR2}}_{\mathrm{VBF}}(m_{jj}) \tag{3}$$

$N^{\mathrm{CR1}}_{\mathrm{QCD}}$(central) is defined as the yield observed in a sample of events with a LS $\tau_h\tau_h$ pair and no VBF requirements, minus the non-QCD background contribution predicted by MC. The LS signal region is included in that selection, but any signal contamination is found to be negligible. The OS to LS ratio, $R_{\mathrm{OS/LS}}$, is obtained from a low $E_{\mathrm{T}}^{\mathrm{miss}}$ sideband ($E_{\mathrm{T}}^{\mathrm{miss}} < 30$ GeV) by subtracting the contributions of non-QCD processes estimated in simulation from data. The measured ratio is $R_{\mathrm{OS/LS}} = 1.328 \pm 0.033$. Additionally, closure is shown in data by using the previously measured ratio $R_{\mathrm{OS/LS}}$ to extrapolate from LS to OS control regions defined with $E_{\mathrm{T}}^{\mathrm{miss}} < 30$ GeV and two non-isolated τ_hs. The efficiency of the VBF cuts is measured in exclusive sidebands fulfilling inverted τ_h isolation criteria. It is estimated as the rate of events with two non-isolated τ_hs plus two jets passing the VBF requirements divided by the rate of events with two non-isolated τ_hs without additional jet requirements. The measured efficiency is $\epsilon_{\mathrm{VBF}} = 0.35\% \pm 0.08\%(stat.) \pm 0.06\%(syst.)$.

For the LS $\tau_h\tau_h jj$ search channel, the QCD multijet background is estimated using Equation 4, in order to have an independent background estimation from the OS channel.

$$N^{\mathrm{signal}}_{\mathrm{QCD}} = N^{\text{failing VBF}}_{\mathrm{QCD}} \cdot \frac{\epsilon^{\text{non-isolated}\,\tau_h}_{\mathrm{VBF}}}{1 - \epsilon^{\text{non-isolated}\,\tau_h}_{\mathrm{VBF}}} \tag{4}$$

$N^{\text{failing VBF}}_{\mathrm{QCD}}$ is the observed yield in data minus the non-QCD background rates from simulation, in a LS $\tau_h\tau_h$ control region with at least two additional jets failing any of the $\Delta\eta_{jj}$, $\eta_1 \cdot \eta_2$, or m_{jj} requirements.

The VBF efficiency, ϵ_{VBF}, is measured in three exclusive τ_h isolation sidebands, without a $E_{\mathrm{T}}^{\mathrm{miss}}$ cut and at least two jets, for each $\tau_h\tau_h$ charge requirement (six independent measurements). The validity of the method is shown in data by the agreement, within statistical uncertainties, of the six independent measurements of ϵ_{VBF}. Since these measurements are performed in control regions without a $E_{\mathrm{T}}^{\mathrm{miss}}$ cut and requiring exclusively different variants of τ_h isolation, the MC simulated samples are also used to test the stability of ϵ_{VBF} as a function of $E_{\mathrm{T}}^{\mathrm{miss}}$ and τ_h isolation. For this purpose, the probability for a single jet to be misidentified as a τ_h is determined in simulation. The misidentification rates for each jet depend on p_T and are used to determine an overall weight, which is applied to each event. The event weights are assigned according to a randomly selected permutation of two jets being redefined as τ_hs. The VBF efficiencies in simulation are calculated from these weighted samples and show stability with respect to the $E_{\mathrm{T}}^{\mathrm{miss}}$ and τ_h isolation requirements at the level of $\sim$ 19%, which is used to assign a systematic uncertainty on the final data-driven QCD multijet background prediction. Finally, the extrapolation efficiency from $\tau_h^{\pm}\tau_h^{\pm}jj$ failing VBF selections to $\tau_h^{\pm}\tau_h^{\pm}jj$ passing VBF selections is $\epsilon_{\mathrm{VBF}} = 6.7\% \pm 0.5\%(stat.)^{+1.2\%}_{-0.5\%}(syst.)$.

7 Systematic Uncertainties

The main contributions to the total systematic uncertainty on the background predictions are from the closure tests and statistical uncertainties of the data used in the control regions for measuring $\epsilon_{\mathrm{VBF}}^{\mathrm{CR}}$, $SF_{\mathrm{central}}^{\mathrm{CR}}$, and $R_{\mathrm{OS/LS}}$. The systematic uncertainties on $SF_{\mathrm{central}}^{\mathrm{CR}}$ and $R_{\mathrm{OS/LS}}$ due to statistics in the CRs are in the range of 1 to 25%, depending on the background and search channel. For $m_{jj} > 250$ GeV, the statistical uncertainties on $\epsilon_{\mathrm{VBF}}^{\mathrm{CR}}$ are in the range of 3 to 21%, while the systematic uncertainties on the background prediction resulting from closure tests performed with simulation and data range from $\sim$ 2% to 20%.

The smaller contributions to the systematic uncertainties on the background predictions include the contamination from other backgrounds in the control regions used to measure $\epsilon_{\mathrm{VBF}}^{\mathrm{CR}}$ as well as the uncertainties on $SF_{\mathrm{central}}^{\mathrm{CR}}$ due to lepton identification efficiency, lepton energy and momentum scale, $E_{\mathrm{T}}^{\mathrm{miss}}$ scale, and trigger efficiency. The contamination from other backgrounds in the control regions has a negligible effect on the systematic uncertainty.

The efficiencies for electron/muon reconstruction and identification are measured with the "tag-and-probe" method [20, 21] with a resulting uncertainty of 2%. The τ_h trigger and identification efficiencies are measured from a fit to the $Z \to \tau\tau \to \mu\tau_h$ visible mass distribution of a sample selected by single-muon triggers, leading to a relative uncertainty of 6% per τ_h candidate [33]. The $E_{\mathrm{T}}^{\mathrm{miss}}$ scale uncertainties contribute via the jet energy scale (2-10% depending on η and p_{T}) and unclustered energy scale (10%), where unclustered energy is defined as the energy not associated with the reconstructed leptons and jets with $p_{\mathrm{T}} > 10\,\mathrm{GeV}$.

Since the estimation of the background contributions in the signal region is partly based on simulation, due to the data-to-simulation correction factors for the efficiency of the central selections, both the signal and background are affected by similar sources of systematic uncertainties. For example, the uncertainty in the luminosity measurement is 2.6% [34] and affects both the signal and background. The uncertainty in the lepton identification efficiency, lepton energy/momentum scale, $E_{\mathrm{T}}^{\mathrm{miss}}$ scale, and trigger efficiency also contribute to the systematic uncertainty on signal. The unclustered energy scale uncertainty has a negligible systematic effect on the signal acceptance.

The experimental acceptance for the VBF selections in signal events depends on the reconstruction/identification efficiency and jet energy scale of forward jets. The jet identification

efficiency is $> 98\%$ for the entire η and p_T range and is validated by observing agreement between data and simulation in the η distribution of jets, in particular at high η, in control samples enriched with $t\bar{t}$ background events. The dominant uncertainty on signal acceptance is due to the modeling of the jet energy scale, and thus the VBF efficiency, for forward jets in MADGRAPH. This is investigated by comparing the predicted and measured m_{jj} spectra in the Z + jets CRs. The level of agreement between the predicted and observed m_{jj} spectra is $< 23\%$, and is treated as a systematic uncertainty on the VBF efficiency for signal samples. The uncertainty on signal acceptance due to the PDF set included in the simulated samples is evaluated in accordance with the PDF4LHC recommendations by comparing CTEQ6.6L, MRST2006, and NNPDF10 PDF sets [35–37] with the default PDF set (CTEQ 6L). The dominant uncertainties that contribute to the m_{jj} shape variations include the $E_{\mathrm{T}}^{\mathrm{miss}}$ and jet energy scale uncertainties.

8 Results

Figures 1 and 2 show the observed and predicted background m_{jj} spectrum in the signal region, obtained using the CRs and methods discussed above. Figure 3(b) shows the combination of the eight search channels. Tables 1 and 2 show a more detailed breakdown of the predicted background rates and observed number of events for the OS and LS channels for all the different final states. The uncertainties quoted are the combination of statistical uncertainties in data and simulation.

Table 1: Number of observed events in data and estimated background rates for the OS search channels. The uncertainties are based on the number of observed events in the CRs as well as the statistics in simulation.

Process	$\mu^{\pm}\mu^{\mp}jj$	$\mathrm{e}^{\pm}\mu^{\mp}jj$	$\mu^{\pm}\tau_h^{\mp}jj$	$\tau_h^{\pm}\tau_h^{\mp}jj$
DY + jets	4.3 ± 1.7	$3.7\pm^{2.1}_{1.9}$	19.9 ± 2.9	12.3 ± 4.4
W + jets	< 0.01	$4.2\pm^{3.3}_{2.5}$	17.3 ± 3.0	2.0 ± 1.7
VV	2.8 ± 0.5	3.1 ± 0.7	2.9 ± 0.5	0.5 ± 0.2
$t\bar{t}$	24.0 ± 1.7	$19.0\pm^{2.3}_{2.4}$	11.7 ± 2.8	–
QCD	–	–	–	6.3 ± 1.8
Higgs	1.0 ± 0.1	1.1 ± 0.5	–	1.1 ± 0.1
VBF Z	–	–	–	0.7 ± 0.2
Total	32.2 ± 2.4	$31.1\pm^{4.6}_{4.1}$	51.8 ± 5.1	22.9 ± 5.1
Observed	31	22	41	31

The observed number of events in the signal regions do not reveal any evidence for new physics. To quantify the sensitivity of this search, the results are presented in the context of the R-parity conserving Minimal Supersymmetric Standard Model (MSSM) and considering production of charginos and neutralinos with two associated jets, as described in section 4. SUSY models with bino-like $\tilde{\chi}_1^0$ and wino-like $\tilde{\chi}_2^0$ and $\tilde{\chi}_1^{\pm}$ are considered. Since the latter two gauginos belong to the same gauge group multiplet, we set $m_{\tilde{\chi}_2^0} = m_{\tilde{\chi}_1^{\pm}}$ and present results as a function of this common mass and the LSP mass $m_{\tilde{\chi}_1^0}$. In the presence of a light slepton, $\tilde{l} = \tilde{e}/\tilde{\mu}/\tilde{\tau}$, it is likely that $\tilde{\chi}_1^{\pm}$ will decay to $l\nu\tilde{\chi}_1^0$ and $\tilde{\chi}_2^0$ to $l^+l^-\tilde{\chi}_1^0$. The results are interpreted by considering $\tilde{l} = \tilde{\tau}_1$ and assuming $B(\tilde{\chi}_2^0 \to \tau\tilde{\tau} \to \tau\tau\tilde{\chi}_1^0) = 1$ and $B(\tilde{\chi}_1^{\pm} \to \nu\tilde{\tau} \to \nu\tau\tilde{\chi}_1^0) = 1$. To highlight how the VBF searches described in this paper complement other searches for electroweak SUSY, three scenarios are considered: (i) $m_{\tilde{\chi}_1^0} = 0$ GeV (large mass gaps), (ii) $m_{\tilde{\chi}_1^0} = 50$ GeV and (iii) $m_{\tilde{\chi}_1^{\pm}} - m_{\tilde{\chi}_1^0} = 50$ GeV (compressed spectra).

The signal acceptance is summarized in Table 3. Since the e, μ and τ_h are characterized by

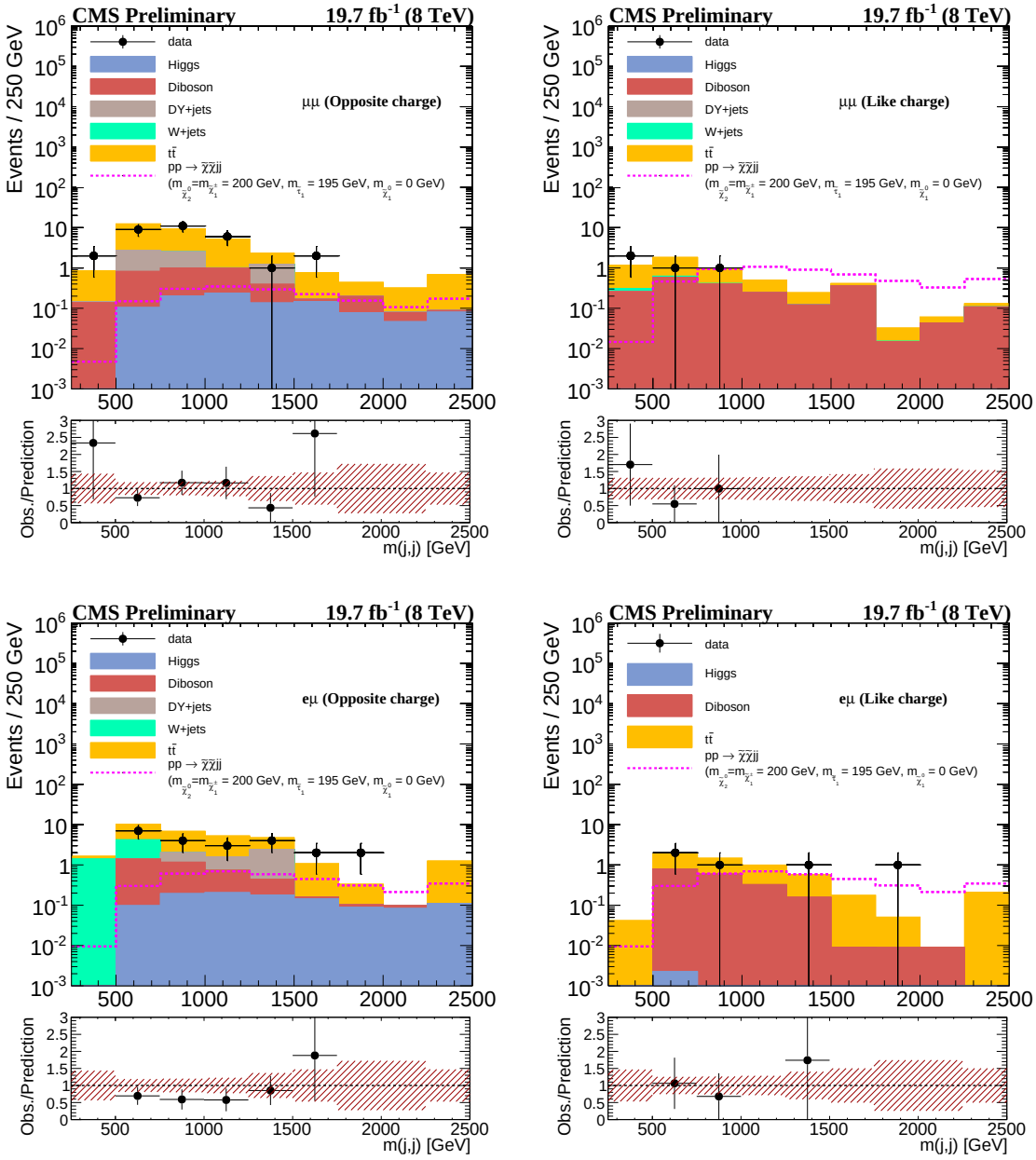

Figure 1: $m(j,j)$ distributions in the (a) OS $\mu\mu$, (b) LS $\mu\mu$, (c) OS eμ, and (d) LS eμ signal regions. The signal scenario with $m_{\tilde{\chi}_2^0} = m_{\tilde{\chi}_1^\pm} = 200$ GeV, $m_{\tilde{\tau}_1} = 195$ GeV, and $m_{\tilde{\chi}_1^0} = 0$ GeV is shown. The shaded band in the ratio plot corresponds to the systematic uncertainty on the background prediction.

softer p_T than in models with prompt production of e/μ, due to the associated neutrinos in the decay of τ leptons, the $p_T(\mathrm{e}/\mu) > 30$ GeV and $p_T(\tau_h) > 45$ GeV requirements defining the search regions result in at least one "lost e/μ/τ_h" (i.e. not passing the object reconstruction and identification criteria) in processes such as $\tilde{\chi}_1^\pm \tilde{\chi}_2^0 jj$ which produce $> 2\tau$ leptons. Therefore, the signal acceptance is similar for the OS and LS channels defined by similar signal selections. For the $\mu\mu jj$ channel, the acceptance is presented for the "Tight" and "Loose" event selection criteria, as explained in section 5.

The expected signal yields predicted from simulation with $m_{\tilde{\chi}_1^0} = 0$ GeV, $m_{\tilde{\chi}_1^0} = 50$ GeV and

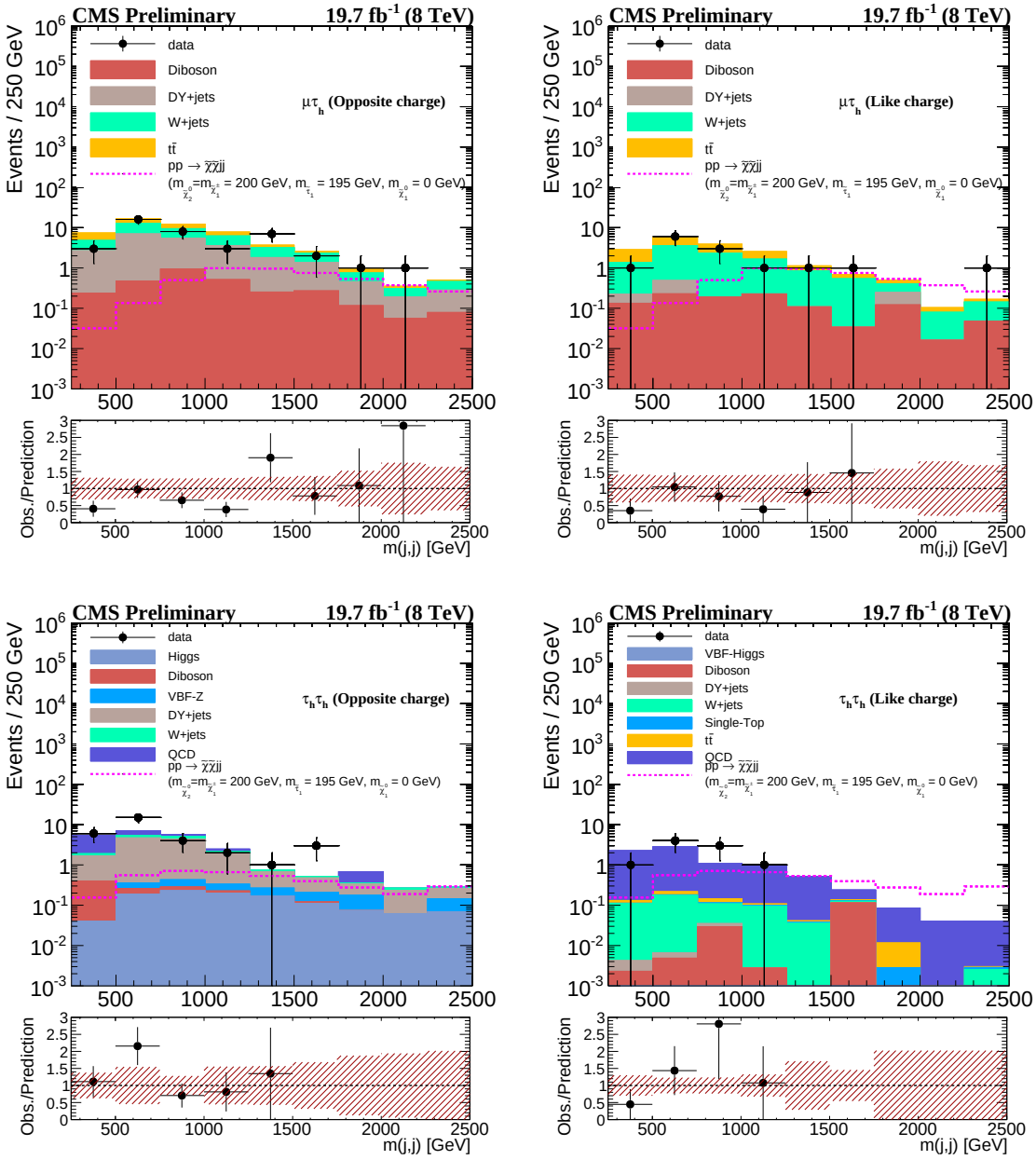

Figure 2: $m(j,j)$ distributions in the (a) OS $\mu\tau_h$, (b) LS $\mu\tau_h$, (c) OS $\tau_h\tau_h$, and (d) LS $\tau_h\tau_h$ signal regions. The signal scenario with $m_{\tilde{\chi}_2^0} = m_{\tilde{\chi}_1^\pm} = 200$ GeV, $m_{\tilde{\tau}_1} = 195$ GeV, and $m_{\tilde{\chi}_1^0} = 0$ GeV is shown. The shaded band in the ratio plot corresponds to the systematic uncertainty on the background prediction.

$\Delta m(\tilde{\chi}_1^\pm, \tilde{\chi}_1^0) = 50$ GeV, are presented in Table 4. In general, the signal acceptance depends on the mass $m_{\tilde{\tau}_1}$ of the intermediate slepton, which is often parameterized in terms of the variable $x_{\tilde{\tau}_1}$ as:

$$m_{\tilde{\tau}_1} = m_{\tilde{\chi}_1^0} + x_{\tilde{\tau}_1}(m_{\tilde{\chi}_1^\pm} - m_{\tilde{\chi}_1^0}) \tag{5}$$

where $0 < x_{\tilde{\tau}_1} < 1$. The expected signal yields in Table 4 are shown for two slepton definitions: (i) using a fixed $\Delta m(\tilde{\chi}_1^\pm, \tilde{\tau}) = 5$ GeV, and (ii) with $x_{\tilde{\tau}_1} = 0.50$. For example, in the compressed

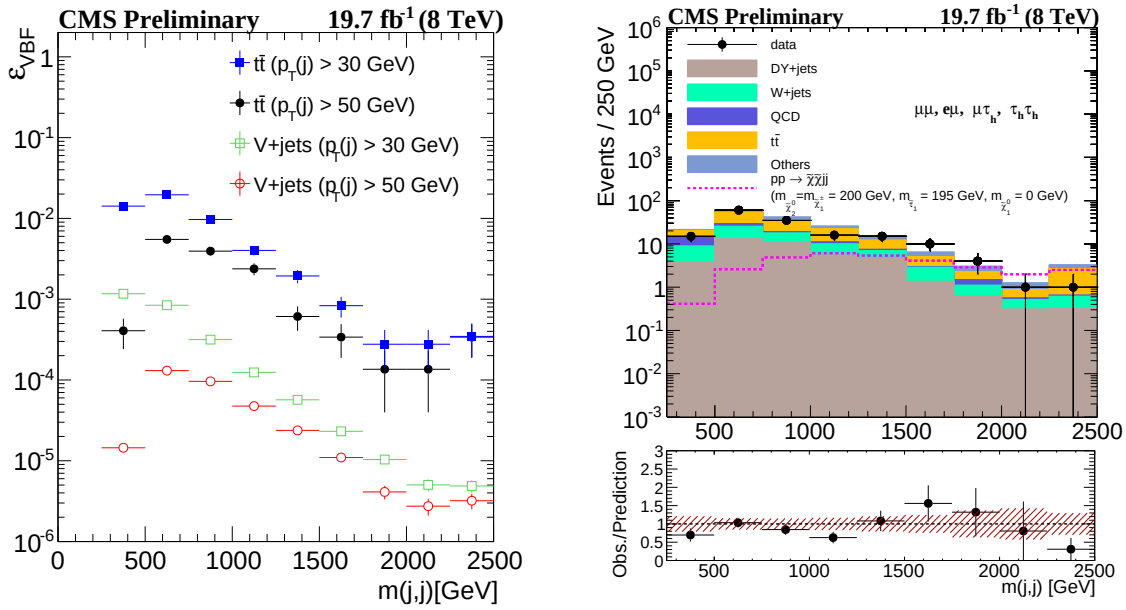

Figure 3: (a) m_{jj} efficiencies for the Z and $t\bar{t}$ CRs of the $\mu\mu jj$ final state. (b) m_{jj} signal region distribution for the combination of all search channels. The signal scenario with $m_{\tilde{\chi}_2^0} = m_{\tilde{\chi}_1^\pm} =$ 200 GeV, $m_{\tilde{\tau}_1} = 195$ GeV, and $m_{\tilde{\chi}_1^0} = 0$ GeV is shown. The shaded band in the ratio plot corresponds to the systematic uncertainty on the background prediction.

Table 2: Number of observed events in data and estimated background rates for the LS channels. The uncertainties are based on the number of observed events in the CRs as well as the statistics in simulation.

Process	$\mu^\pm\mu^\pm jj$	$e^\pm\mu^\pm jj$	$\mu^\pm\tau_h^\pm jj$	$\tau_h^\pm\tau_h^\pm jj$
DY + jets	< 0.01	$0\pm^{1.7}_{0}$	0.5 ± 0.2	< 0.01
W + jets	$0.1 \pm 8.2 \times 10^{-4}$	$0\pm^{3.0}_{0}$	9.3 ± 2.3	0.5 ± 0.1
VV	2.1 ± 0.3	$1.9\pm^{0.4}_{0.2}$	1.1 ± 0.2	$0.1 \pm 6.5 \times 10^{-2}$
$t\bar{t}$	3.1 ± 0.1	$3.5\pm^{0.7}_{0.9}$	6.7 ± 2.8	$0.1 \pm 1.2 \times 10^{-2}$
Single top	–	–	–	< 0.1
QCD	–	–	–	7.6 ± 0.9
Higgs	–	–	–	< 0.01
Total	5.4 ± 0.3	$5.4\pm^{3.5}_{0.9}$	17.6 ± 3.8	8.4 ± 0.9
Observed	4	5	14	9

mass-spectra scenario of $m_{\tilde{\chi}_1^\pm} - m_{\tilde{\chi}_1^0} = 50$ GeV, a slepton mass equal to the mean of the LSP and the $\tilde{\chi}_1^\pm/\tilde{\chi}_2^0$ masses ($x_{\tilde{\tau}_1} = 0.50$) results in a significantly lower average p_T for the leptons produced by the $\tilde{\tau}_1$ decays. As a consequence, the acceptance is reduced with respect to the $m_{\tilde{\chi}_1^\pm} - m_{\tilde{\tau}_1} = 5$ GeV scenario by a factor between 2 and 3. On the other hand, in the maximal mass gap scenario with $m_{\tilde{\chi}_1^0} = 0$ GeV, a slepton mass equal to the mean of the LSP and the $\tilde{\chi}_1^\pm/\tilde{\chi}_2^0$ masses results in more significant values of p_T for all leptons, leading to a signal acceptance that is $\sim 1.25 - 1.75$ times that of the $m_{\tilde{\chi}_1^\pm} - m_{\tilde{\tau}_1} = 5$ GeV scenario.

The calculation of the exclusion limit is obtained by using the m_{jj} distribution per channel to construct a combined likelihood in bins of m_{jj} and computing the 95% confidence level (CL) up-

Table 3: Cumulative signal acceptance for $m_{jj} > 250$ GeV.

channel	BR($\geq 1\ell_1$ & $\geq 1\ell_2$)	ll+MET	VBF
$\mu^+\tau_h^-$ ($\mu^\pm\tau_h^\pm$)	0.399	0.0197 (0.0196)	0.0075 (0.0074)
$e^+\mu^-$ ($e^\pm\mu^\pm$)	0.152	0.0367 (0.0373)	0.0140 (0.0140)
$\tau_h^+\tau_h^-$ ($\tau_h^\pm\tau_h^\pm$)	0.717	0.0098 (0.0097)	0.0092 (0.0093)
$\mu^+\mu^-$ ($\mu^\pm\mu^\pm$)	0.081	0.0181 (0.0180)	0.0070 (0.0172)

Table 4: Simulated yield of signal events. The terms in only curly brackets, $\{m_{\tilde{\chi}_1^\pm}, m_{\tilde{\tau}}\}$, represent the scenarios where $\Delta m(\tilde{\chi}_1^\pm, \tilde{\tau}) = 5$ GeV, while the terms in parenthesis, ($\{m_{\tilde{\chi}_1^\pm}, m_{\tilde{\tau}}\}$), are for scenarios where $m(\tilde{\tau}_1) = \frac{1}{2}m(\tilde{\chi}_1^0) + \frac{1}{2}m(\tilde{\chi}_1^\pm)$.

$\{m(\tilde{\chi}_1^\pm)$,$m(\tilde{\tau})\}$ [GeV]	$\mu^\pm\mu^\pm jj$ (Loose)	$\mu^\pm\mu^\mp jj$ (Tight)	eμjj	$\mu\tau_h jj$	$\tau_h\tau_h jj$
$m(\tilde{\chi}_1^0) = 0$ GeV					
{100, 95} ({100, 50})	16.22(28.94)	6.61(11.79)	13.21(23.57)	7.10(9.36)	8.65(10.73)
{200, 195} ({200, 100})	5.42(9.67)	1.76(3.14)	3.52(6.28)	4.53(5.97)	3.76(4.67)
{300, 295} ({300, 150})	2.27(4.05)	0.68(1.21)	1.37(2.44)	1.85(2.54)	1.53(2.04)
{400, 395} ({400, 200})	0.57(1.02)	0.17(3.03)	0.35(0.62)	0.46(0.63)	0.38(0.51)
$m(\tilde{\chi}_1^0) = 50$ GeV					
{100, 95} ({100, 75})	5.66(2.21)	3.30(1.29)	6.60(2.58)	4.34(1.51)	2.07(0.41)
{200, 195} ({200, 125})	3.03(5.41)	1.11(1.98)	2.21(3.94)	3.06(4.04)	2.41(2.99)
{300, 295} ({300, 175})	1.27(2.27)	0.60(1.07)	1.19(2.12)	1.66(2.28)	1.40(1.86)
{400, 395} ({400, 225})	0.34(0.61)	0.16(0.29)	0.32(0.57)	0.43(0.59)	0.36(0.48)
$\Delta m(\tilde{\chi}_1^\pm - \tilde{\chi}_1^0) = 50$ GeV					
{200, 195} ({200, 175})	1.38(0.54)	0.85(0.33)	1.65(0.65)	0.99(0.35)	0.46(0.09)
{300, 295} ({300, 275})	0.47(0.18)	0.28(0.11)	0.58(0.23)	0.40(0.14)	0.20(0.04)
{400, 395} ({400, 375})	0.12(0.05)	0.08(0.03)	0.15(0.06)	0.10(0.03)	0.05(0.01)

per limit on the signal cross section using the CL_s method [38]. Systematic uncertainties are represented by nuisance parameters, which we remove by marginalization, assuming a gamma or log normal prior for normalization parameters, and Gaussian priors for mass-spectrum shape uncertainties. The combination of the eight search channels require simultaneous analysis of the data from all individual search channels, accounting for all statistical and systematic uncertainties and their correlations.

Figures 4(a) and (b), show the expected and observed limits as well as the theoretical cross section as functions of $m_{\tilde{\chi}_1^\pm}$ for the models where $\Delta m(\tilde{\chi}_1^\pm, \tilde{\tau}) = 5$ GeV and $x_{\tilde{\tau}_1} = 0.50$, respectively. We exclude $\tilde{\chi}_2^0/\tilde{\chi}_1^\pm$ with masses below 300 GeV, conservatively using the -1σ theoretical cross section, for the mass spectra scenario with $x_{\tilde{\tau}_1} = 0.50$ and $m_{\tilde{\chi}_1^0} = 0$. The bound is $m_{\tilde{\chi}} = 170$ GeV for the compressed mass spectra scenario of $m_{\tilde{\chi}_1^\pm} - m_{\tilde{\chi}_1^0} = 50$ GeV and $\Delta m(\tilde{\chi}_1^\pm, \tilde{\tau}) = 5$ due to the softer lepton p_T spectrum.

9 Summary

A search is performed for non-colored supersymmetric particles with the VBF topology using data corresponding to an integrated luminosity of 19.7 fb^{-1} collected by the CMS detector in proton-proton collisions at $\sqrt{s} = 8$ TeV. It is the first search for supersymmetry with the VBF topology. The VBF analysis to search for SUSY using muon and τ_h triggers is presented in eight different search regions containing pairs of leptons with same-sign or opposite-sign electric charge. The observed m_{jj} distributions do not reveal any evidence for new physics. The results are used to exclude a range of $\tilde{\chi}_1^\pm/\tilde{\chi}_2^0$ masses up to 300 GeV, at 95% CL, in the context of models

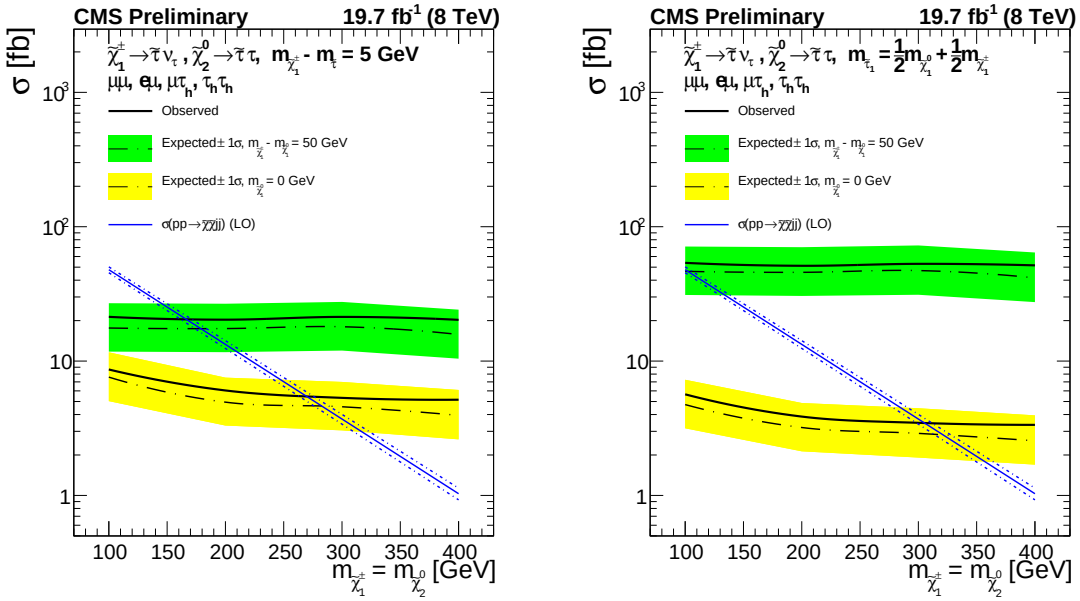

Figure 4: Combined 95% CL upper limits on the cross section as a function of $m_{\tilde{\chi}_2^0} = m_{\tilde{\chi}_1^\pm}$. The left figure shows the upper limits for the scenario where $m_{\tilde{\tau}}$ is defined as $m_{\tilde{\chi}_1^\pm} - m_{\tilde{\tau}} = 5$, for two different $m_{\tilde{\chi}_1^0}$ definitions: $m_{\tilde{\chi}_1^\pm} - m_{\tilde{\chi}_1^0} = 50$ (compressed spectra) and $m_{\tilde{\chi}_1^0} = 0$ GeV (large mass gap). The right figure shows the upper limits for the scenarios where $m_{\tilde{\tau}}$ is defined as $m(\tilde{\tau}_1) = \frac{1}{2}m(\tilde{\chi}_1^0) + \frac{1}{2}m(\tilde{\chi}_1^\pm)$, for the same two $m_{\tilde{\chi}_1^0}$ definitions.

that assume large mass gaps ($m_{\tilde{\chi}_1^0} = 0\,\text{GeV}$) and large branching fractions of $\tilde{\chi}_1^\pm/\tilde{\chi}_2^0$ to τ leptons. The results are also used to exclude $m_{\tilde{\chi}} < 170$ GeV for the compressed mass spectra scenario of $m_{\tilde{\chi}_1^\pm} - m_{\tilde{\chi}_1^0} = 50$ GeV. While a number of previous studies at the LHC have focused on strongly coupled supersymmetric particles and Drell-Yan production of the electroweak sector of supersymmetry in multilepton final states, this analysis produces the most stringest limits to date on the production of charginos and neutralinos decaying to τ leptons in compressed mass spectra scenarios defined by mass separation $\Delta m = m_{\tilde{\chi}_1^\pm} - m_{\tilde{\chi}_1^0} < 50$ GeV.

Acknowledgements

We congratulate our colleagues in the CERN accelerator departments for the excellent performance of the LHC machine. We thank the technical and administrative staff at CERN and other CMS institutes, and acknowledge support from: FMSR (Austria); FNRS and FWO (Belgium); CNPq, CAPES, FAPERJ, and FAPESP (Brazil); MES (Bulgaria); CERN; CAS, MoST, and NSFC (China); COLCIENCIAS (Colombia); MSES (Croatia); RPF (Cyprus); MoER, SF0690030s09 and ERDF (Estonia); Academy of Finland, MEC, and HIP (Finland); CEA and CNRS/IN2P3 (France); BMBF, DFG, and HGF (Germany); GSRT (Greece); OTKA and NKTH (Hungary); DAE and DST (India); IPM (Iran); SFI (Ireland); INFN (Italy); NRF and WCU (Korea); LAS (Lithuania); CINVESTAV, CONACYT, SEP, and UASLP-FAI (Mexico); MSI (New Zealand); PAEC (Pakistan); MSHE and NSC (Poland); FCT (Portugal); JINR (Armenia, Belarus, Georgia, Ukraine, Uzbekistan); MON, RosAtom, RAS and RFBR (Russia); MSTD (Serbia); MICINN and CPAN (Spain); Swiss Funding Agencies (Switzerland); NSC (Taipei); TUBITAK and TAEK (Turkey); STFC (United Kingdom); DOE and NSF (USA).

Individuals have received support from the Marie-Curie programme and the European

Research Council and EPLANET (European Union); the Leventis Foundation; the A. P. Sloan Foundation; the Alexander von Humboldt Foundation; the Belgian Federal Science Policy Office; the Fonds pour la Formation à la Recherche dans l'Industrie et dans l'Agriculture (FRIA-Belgium); the Agentschap voor Innovatie door Wetenschap en Technologie (IWT-Belgium); the Ministry of Education, Youth and Sports (MEYS) of the Czech Republic; the Council of Science and Industrial Research, India; the HOMING PLUS programme of the Foundation for Polish Science, cofinanced from European Union, Regional Development Fund; the Compagnia di San Paolo (Torino); the Consorzio per la Fisica (Trieste); MIUR project 20108T4XTM (Italy); the Thalis and Aristeia programmes cofinanced by EU-ESF and the Greek NSRF; and the National Priorities Research Program by Qatar National Research Fund.

References

[1] CMS Collaboration, "Search for new physics in the multijet and missing transverse momentum final state in proton-proton collisions at $\sqrt{s} = 8$ TeV", *J. High Energy Phys.* **06** (2014) 55.

[2] ATLAS Collaboration, "Search for new phenomena in final states with large jet multiplicities and missing transverse momentum at $\sqrt{s} = 8$ TeV", *J. High Energy Phys.* **10** (2014) 130.

[3] CMS Collaboration, "Search for new physics in events with same-sign dileptons and jets in pp collisions at $\sqrt{s}$ = 8 TeV", *JHEP* **1401** (2014) 163, doi:10.1007/JHEP01(2015)014,10.1007/JHEP01(2014)163, arXiv:1311.6736.

[4] CMS Collaboration, "Search for physics beyond the standard model in events with two leptons, jets, and missing transverse momentum in pp collisions at sqrt(s) = 8 TeV", arXiv:1502.06031.

[5] ATLAS Collaboration, "Search for supersymmetry at $\sqrt{s}$=8 TeV in final states with jets and two same-sign leptons or three leptons with the ATLAS detector", *JHEP* **1406** (2014) 035, doi:10.1007/JHEP06(2014)035, arXiv:1404.2500.

[6] CMS Collaboration, "Searches for electroweak production of charginos, neutralinos, and sleptons decaying to leptons and W,Z, and Higgs bosons in pp collisions at 8 TeV", *EPJC* **74** (2014) 3036, doi:10.1140/epjc/s10052-014-3036-7.

[7] ATLAS Collaboration, "Search for direct production of charginos and neutralinos in events with three leptons and missing transverse momentum in $\sqrt{s} = 8$TeV pp collisions with the ATLAS detector", *JHEP* **1404** (2014) 169, doi:10.1007/JHEP04(2014)169, arXiv:1402.7029.

[8] B. Dutta et al., "Vector boson fusion processes as a probe of supersymmetric electroweak sectors at the LHC", *Phys. Rev. D* **87** (2013) 035029.

[9] A. G. Delannoy et al., "Probing Dark Matter at the LHC Using Vector Boson Fusion Processes", *Phys. Rev. Lett.* **111** (Aug, 2013) 061801, doi:10.1103/PhysRevLett.111.061801.

[10] CMS Collaboration, "Search for an Invisible Higgs Boson", *CMS Physics Analysis Summary* **CMS-PAS-HIG-13-013** (2013).

[11] CMS Collaboration, "Update of the search for the Standard Model Higgs boson decaying into WW in the vector boson fusion production channel", *CMS Physics Analysis Summary* **CMS-PAS-HIG-13-022** (2013).

[12] "Studies of the VBF $H \to \tau_l \tau_{had}$ analysis at High Luminosity LHC conditions", Technical Report ATL-PHYS-PUB-2014-018, CERN, Geneva, Oct, 2014.

[13] CMS Collaboration, "The CMS experiment at the CERN LHC", *JINST* **03** (2008) S08004, doi:10.1088/1748-0221/3/08/S08004.

[14] CMS Collaboration, "Commissioning of the Particle-Flow Reconstruction in Minimum-Bias and Jet Events from pp Collisions at 7 TeV", CMS Physics Analysis Summary CMS-PAS-PFT-10-002, 2010.

[15] M. Cacciari, G. P. Salam, and G. Soyez, "The Anti-k(t) jet clustering algorithm", *J. High Energy Phys.* **04** (2008) 063, doi:10.1088/1126-6708/2008/04/063, arXiv:0802.1189.

[16] CMS Collaboration, "Pileup Jet Identification", Technical Report CMS-PAS-JME-13-005, CERN, Geneva, 2013.

[17] CMS Collaboration, "Determination of jet energy calibration and transverse momentum resolution in CMS", *JINST* **6** (2011) 11002, doi:10.1088/1748-0221/6/11/P11002, arXiv:1107.4277.

[18] CMS Collaboration, "b-jet Identification in the CMS Experiment", CMS Physics Analysis Summary PAS BTV-11-004, 2012.

[19] CMS Collaboration, "Performance of b tagging at $\sqrt{s}$=8 TeV in multijet, $t\bar{t}$ and boosted topology events", CMS Physics Analysis Summary PAS BTV-13-001, 2013.

[20] CMS Collaboration, "Performance of muon identification in pp collisions at $\sqrt{s} = 7$ TeV", *JINST* **07** (2012) P10002, doi:10.1088/1748-0221/7/10/P10002.

[21] CMS Collaboration, "Electron reconstruction and identification at $\sqrt{s} = 7$ TeV", CMS Physics Analysis Summary CMS-PAS-EGM-10-004, 2010.

[22] CMS Collaboration, "Single Muon efficiencies in 2012 Data", Technical Report CMS-DP-2013-009, CERN, Geneva, 2013.

[23] CMS Collaboration, "Muon Identification performance: hadron mis-Id measurements and RPC Muon selections", Technical Report CMS-DP-2014-018, CERN, Geneva, 2014.

[24] CMS Collaboration, "Electron performance with 19.6 fb^{-1} of data collected at $\sqrt{s} = 8$ TeV with the CMS detector.", Technical Report CMS-DP-2013-003, CERN, Geneva, 2013.

[25] CMS Collaboration, "Performance of τ-lepton reconstruction and identification in CMS", *JINST.* **07** (2012) P01001, doi:10.1088/1748-0221/7/01/P01001.

[26] CMS Collaboration, "Tau ID Performance Plots", Technical Report CMS-DP-2014-015, CERN, Geneva, 2014.

[27] J. Alwall, "MadGraph/MadEvent v4: The New Web Generation", *J. High Energy Phys.* **09** (2008) 028, doi:10.1088/1126-6708/2007/09/028, arXiv:0706.2334.

[28] S. Frixion et al., "Matching NLO QCD computations with parton shower simulations: the POWHEG method", *J. High Energy Phys.* **11** (2007) 070, doi:10.1088/1126-6708/2007/11/070.

[29] T. Sjöstrand, S. Mrenna, and P. Z. Skands, "PYTHIA 6.4 Physics and Manual", *J. High Energy Phys.* **05** (2006) 026, doi:10.1088/1126-6708/2006/05/026, arXiv:hep-ph/0603175.

[30] Z. Was et al., "TAUOLA the library for tau lepton decay", *Nucl. Phys. B Proc. Suppl.* **98** (2001) 96, doi:10.1016/S0920-5632(01)01200-2, arXiv:hep-ph/0011305.

[31] GEANT4 Collaboration, "GEANT4: A Simulation toolkit", *Nucl. Instrum. Meth.* **A506** (2003) 250, doi:10.1016/S0168-9002(03)01368-8.

[32] CMS Collaboration, "The fast simulation of the CMS detector at LHC", *J. Phys. Conf. Ser.* **331** (2011) 032049, doi:doi:10.1088/1742-6596/331/3/032049.

[33] CMS Collaboration, "Measurement of the inclusive Z cross section via decays to tau pairs in pp collisions at $\sqrt{s} = 7$ TeV", *J. High Energy Phys.* **01** (2011) 80, doi:10.1007/JHEP08(2011)117.

[34] CMS Collaboration, "Absolute calibration of the luminosity measurement at CMS: Winter 2012 update", CMS Physics Analysis Summary CMS-PAS-SMP-12-008, 2012.

[35] P. Nadolsky et al., "Implications of CTEQ global analysis for collider observables", *Phys. Rev. D* **78** (2008) 013004, doi:10.1103/PhysRevD.78.013004.

[36] A. D. Martin, W. J. Stirling, R. S. Thorne, and G. Watt, "Update of parton distributions atNNLO", *Phys. Lett. B* **652** (2007) 292, doi:10.1016/j.physletb.2007.07.040.

[37] M. Ubiali, "NNPDF1.0 parton set for the LHC", *Nucl. Phys. Proc. Suppl.* **186** (2009) 62, doi:10.1016/j.nuclphysbps.2008.12.020.

[38] A. L. Read, ".Presentation of search results: the CLS technique", *J. Phys. G* **28** (2002) 2693, doi:doi:10.1088/0954-3899/28/10/313.